J Mater Sci (2019) 54:11243–11253

Materials for life sciences

In vitro preparation and characterization of amorphous calcium carbonate nanoparticles for applications in curcumin delivery

Chaohui Rao[1,2], Xia Guo[1,2], Min Li[1,2], Xiaoqing Sun[1,2], Xiaojie Lian[3], Huifang Wang[1], Xianghua Gao[1,2], Baolong Niu[1,2,*], and Wenfeng Li[1,2,*]

[1] *Key Laboratory of Interface Science and Engineering in Advanced Materials, Taiyuan University of Technology, Ministry of Education, Taiyuan 030024, People's Republic of China*

[2] *College of Materials Science and Engineering, Taiyuan University of Technology, Taiyuan 030024, People's Republic of China*

[3] *College of Biomedical Engineering, Taiyuan University of Technology, Taiyuan 030024, People's Republic of China*

Received: 21 February 2019
Accepted: 7 May 2019
Published online: 13 May 2019

ABSTRACT

The development of high drug loading and sustained release nanoparticles by simple and economical methods is significant for the treatment of diseases. Amorphous calcium carbonate (ACC) is an ideal drug delivery system because of its excellent pH responsiveness, biocompatibility and biodegradability. In this work, ACC nanoparticles were successfully precipitated in ethanol–calcium solutions using ammonium carbonate as the internal source of CO_2, which exhibited a relatively narrow size distribution in range of 10–200 nm. The microscopic morphology, amorphous characters, porous structure and thermal behavior of resultants were investigated by electron microscopy, Fourier-transform infrared spectroscopy, Brunauer–Emmett–Teller and thermogravimetric analysis, respectively. In vitro drug release assay showed that ACC nanoparticles had high loading capacity of curcumin (Cur) and favorable drug release properties. Furthermore, ACC-Cur showed excellent abilities to scavenge free radicals, protect Cur stability and damage A549 cells, providing a broadened space for the applications of this material in the fields of biomedical or food.

Introduction

In the past few decades, many therapeutic strategies such as radiotherapy, chemotherapy and surgery have been developed to overcome the high cancer mortality, in which chemotherapy is currently the most commonly used treatment [1–3]. However, the bioavailability of most anticancer drugs is significantly restricted owing to their poor specificity and chemical instability [4, 5]. Accordingly, numerous

Address correspondence to E-mail: baolongniutyut@hotmail.com; wenfenglityut@live.com

https://doi.org/10.1007/s10853-019-03686-3

nano-sized drug delivery systems such as liposomes, micelles, niosomes and nanobubbles have attracted extensive research interest, which aims to prolong circulation time of anticancer drugs, enhance cellular uptake and reduce toxicity on normal tissue [6–8]. Although these nanocarriers show promising effects in tumor therapy, tedious preparation, complex drug-loading process, unsatisfactory release properties, poor biodegradability and biocompatibility have hindered their applications. Therefore, the development of high drug loading, favorable sustained release and low-toxic nanocarriers using simple and economical methods is a challenge topic in cancer therapy.

Compared with traditional drug delivery nanosystems, the drug carrier based on ACC nanoparticles has many unique properties including excellent pH responsiveness, high loading capacity, ideal biocompatibility and biodegradability, which is favorable for drug delivery in vivo [9–11]. Currently, there are several typical methods to synthesize ACC including channeling CO_2 into solution containing calcium salts, decomposition of dimethyl carbonate in calcium solution by adjusting pH value, as well as rapid mixing of calcium salts and carbonate salts stock solution at low temperatures [12–14]. Although these methods were successfully employed to synthesize ACC, the easy crystallization has hindered the preparation of "pure" ACC nanoparticles in aqueous solution, which is unfavorable for the loading of drugs [14, 15]. Furthermore, though many organic macromolecules and inorganic ions were introduced to control crystallization, they also significantly restricted the synthesis of nano-sized ACC [16, 17].

To synthesize "pure" ACC, a simple method for large-scale preparation of ACC nanoparticles without introduction of additives using ammonium carbonate as carbon source and ethanol as solvent was introduced by Chen et al. [18]. Herein, this strategy was employed in our work for the preparation of "stable" ACC nanoparticles which were applied as a drug delivery system. Before loading the drug, amorphous and crystalline properties of calcium carbonate prepared in various solvents with different ethanol/water volume ratios were analyzed, and the optimum conditions for preparing nano-sized ACC were determined. Meanwhile, multiple techniques were applied to characterize the resultants for evaluating whether this material could be used as a potential drug carrier. Cur has attracted an extensive attention for its applications in cancer therapy and free radicals scavenging [19]. Therefore, it was used as a model drug to study the loading capacity and release properties of ACC nanoparticles in this work. The Cur-loaded ACC (ACC-Cur) showed excellent abilities to scavenge free radicals, protect Cur stability and damage cancer cells, indicating that ACC nanoparticles have promising application in drug delivery.

Experiment

Materials

Calcium chloride, ammonium carbonate, curcumin (Cur, 99%), 1, 1-diphenyl-2-picrylhydrazyl radical (DPPH) and 2, 2-azinobis-(3-ethylbenzothiazoline-6-sulfonic acid) (ABTS) were purchased from Shanghai Aladdin Biochemical Technology Co., Ltd. Absolute ethanol was obtained from Sinopharm Chemical Reagent Co., Ltd. Human lung cancer cells (A549) were provided by Shanghai Cell Bank of the Chinese Academy of Sciences. 3-(4,5-Dimethyl-2-thiazolyl)-2,5-diphenyl-2-*H*-tetrazolium bromide (MTT) was obtained from Beijing Solarbio Science & Technology Co., Ltd. All the other reagents were of analytical grade purity and obtained from commercially available.

Preparation of ACC and Cur-loaded ACC

The synthesis of ACC was performed according to the previous method with some modifications [18]. Briefly, calcium chloride–ethanol mixed solution (10 mM) was prepared in a 100-mL glass beaker and covered by Parafilm with several pores. This beaker was then placed into a bigger glass beaker (500 mL) along with 2 g of ammonium carbonate (Fig. 1a). The suspensions were centrifuged after stirring at 30 °C for 4 h, and the washed solids were freeze-dried prior to analysis. ACC-Cur was prepared using the same method except that Cur (0.5 mg mL^{-1}) and calcium salts were dissolved in absolute ethanol at the same time. The drug-loading content and encapsulation efficiency of Cur were calculated according to the following two equations [16].

$$\text{Drug loading content} = \frac{m_1 - m_2}{m_3} \times 100\% \quad (1)$$

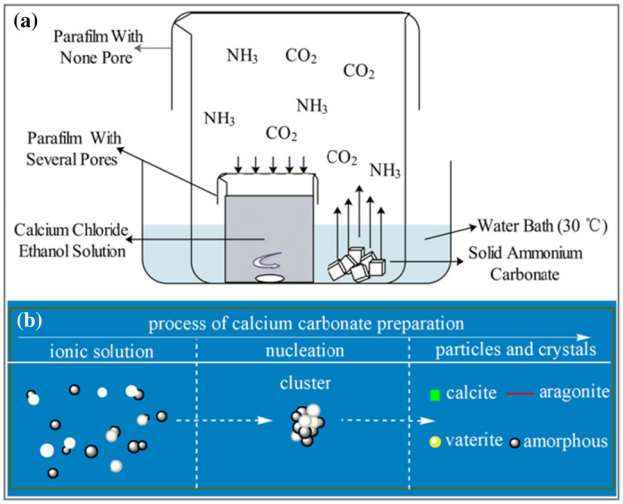

Figure 1 **a** Schematic diagrams: precipitation of ACC nanoparticles in absolute ethanol, **b** the nucleation process of calcium carbonate.

$$\text{Encapsulation efficiency} = \frac{m_1 - m_2}{m_1} \times 100\% \quad (2)$$

where m_1 is the total weight of added-Cur, m_2 is the weight of non-encapsulated Cur, and m_3 is the weight of ACC-Cur.

Characterization

X-ray powder diffraction (XRD) patterns were recorded using X-ray diffractometer (Rigaku D/max 2500 V, Cu Kα radiation, k = 1.54178 Å). The ion concentrations in solution were measured using a multi-parameter analysis instrument (DZS-708L, INESA). Fourier-transform infrared (FT-IR) spectra were taken on a Fourier-transform IR Spectrometer (FTIR-7600, Lambda Scientific, Australia). The concentrations of free Cur were measured by a UV–Vis spectrophotometer (UV-1800, Shimadzu Corporation) in the wavelength range of 300–500 nm. The morphology of ACC was examined by scanning electron microscopy (SEM; Hitachi S-4800, Japan) and transmission electron microscopy (TEM; Hitachi H-800, Japan). The contents of Ca, C and O were recorded by energy-dispersive spectrometer (EDS). Dynamic light scattering (DLS) was applied to measure the diameter of ACC (Malvern, UK). The specific surface area and pore size distribution were measured by the Brunauer–Emmett–Teller (BET; V-Sorb 2800P, Gold APP China) method of N_2 adsorption–desorption at − 196 °C. Thermogravimetric analysis was obtained using a Netzsch TGA-209 under a stream of air at a heating rate of 20 °C min^{-1}.

In vitro drug release assay

The release of Cur was carried out in PBS buffer (pH 5.4 and 7.4) [20]. Briefly, a dialysis bag (34 kDa) containing 10 mg of ACC-Cur and 10 mL of PBS was immersed in 100 mL of PBS and shaken in a water bath at 37 °C. At predetermined intervals, 3 mL of solution was withdrawn from release medium and replaced by 3 mL of fresh PBS. The concentrations of released Cur were determined by UV–Vis spectrophotometer (424 nm).

Determination of antioxidant activity in vitro

The determinations of DPPH and $ABTS^{\cdot+}$ radical scavenging capacity of Cur and ACC-Cur were derived from published protocols [20–22]. Due to solubility differences between Cur and ACC-Cur, the antioxidant capacity of Cur released from ACC-Cur was investigated.

DPPH radical scavenging activity assay

In this assay, 2 mL of various concentrations (0, 2, 4, 6, 8, 10 and 12 μg mL^{-1}) of Cur, ACC-Cur and released Cur were added to 2 mL of DPPH (0.1 mM) ethanol solution. After 30 min of incubation in the dark, the absorbance of mixture was measured at 517 nm. The radical scavenging activity was calculated according to the following equation.

$$\text{Radical scavenging activity} = \frac{A_0 - A_1}{A_0} \times 100\% \quad (3)$$

where A_0 is the absorbance of control group and A_1 is the absorbance of mixtures.

$ABTS^{\cdot+}$ radical scavenging activity assay

The $ABTS^{\cdot+}$ radical cation was generated by mixing 10 mL of ABTS (7 mM) with 10 mL of aqueous potassium persulfate solution (4.9 mM) and then stood the mixture in dark for 12–16 h. Subsequently, the resulting $ABTS^{\cdot+}$ solution was diluted with absolute ethanol to achieve an absorbance of 0.70 ± 0.02 (734 nm). 1 mL of various concentrations (0, 2, 4, 6, 8, 10 and 12 μg mL^{-1}) of Cur, ACC-Cur and released Cur were mixed with 4 mL of $ABTS^{\cdot+}$

solution, and the absorbance of mixture was read (734 nm) after 30 min of incubation in the dark. The free radical scavenging activity was calculated according to Eq. (3).

Cur protection

To elucidate the effect of ACC-encapsulating Cur on its stability, the DPPH free radical scavenging capacity of Cur and ACC-Cur (12 μg mL^{-1}) after thermal treatment (60 °C, 30 min), fluorescent lamp irradiation (FL, 15 W, 1 h), daylight irradiation (1 h) and UV radiation (15 W, 1 h) was assessed [21, 23]. The determination of scavenging capacity of treated ACC-Cur was derived using released Cur.

In vitro cytotoxicity assay

To evaluate toxicity of resultants, the inhibition efficiency of A549 was measured by MTT assay. Cells in medium (DMEM containing 10% FBS) were seeded into 96-well plates and cultured (37 °C) under 5% (v/v) CO_2 atmosphere. After a 24-h incubation period, different concentrations (1, 2, 4, 8, 16 and 32 μg mL^{-1}) of sample solution were added into wells and co-cultured with cells for 24 h. Subsequently, each well was treated with MTT for 4 h and the absorbance of formazan crystals dissolved in DMSO was measured by Microplate Reader (490 nm). The cell viability was calculated according to the following equation [10].

$$\text{Cell viability} = \frac{OD_{treated}}{OD_{control}} \times 100\% \quad (4)$$

where $OD_{treated}$ was obtained from samples-treated cells, and $OD_{control}$ was obtained from control groups.

Statistical analysis

All data were performed in triplicate and presented as averages and standard deviations. One-way analysis of variance (ANOVA) was used for statistical analysis.

Results and discussion

Preparation of ACC nanoparticles

In order to study the amorphous and crystalline characteristics of calcium carbonate prepared in various ethanol/water mixtures, the resultants were characterized by XRD. As shown in Fig. 2a, the blend phase of vaterite and calcite was formed in two solvents with ethanol/water ratios of 1/1 and 1/3 (v/v), while increasing the volume ratio of ethanol to water was favorable for the formation of metastable phase. As expected, the two broad peaks at about 30° and 45° were characteristics of ACC particles synthesized in absolute ethanol. Obviously, the crystallization of ACC was related to the presence of water, which was in accordance with the previous reports [24, 25]. Owing to crystallization kinetics and thermodynamics of calcium carbonate, ACC only exhibits in the initially sedimentary stage and then transforms to a blend of different dehydrated phases before eventually being converted to stable calcite phase (Fig. 1b) [26]. Accordingly, to prepare "pure" ACC for drug transportation, the vapor diffusion method using ethanol as solvent was employed to synthesize this metastable phase.

The optimum calcium concentration for the preparation of ACC was analyzed by XRD. As shown in Fig. 2b, ACC precipitated in low-concentration calcium chloride solutions (10 and 12 mM) was stable, whereas an increased calcium concentration (14 and 16 mM) induced crystallization of resultants. Additionally, in 10 mM calcium chloride solution, the particle size of ACC with positive zeta potential was gradually increased (100–500 nm) with prolonged reaction time, which is listed in Table 1. It was observed that ACC particles exhibit a relatively narrow size distribution located at approximately 100 nm when the reaction time was 4 h (Fig. 3). As we know, due to sustained decomposition of ammonium carbonate for produce of CO_2 and NH_3 gas, the formation of ACC could be considered as a continuous process [18]. Figure 4 shows the tendency of pH and pCa change within the first 1 h, which was measured by multi-parameter analyzer (DZS). With the continuous dissolution of NH_3, the initial solution pH value was about 6.8 before eventually being about 8.4. Meanwhile, Ca^{2+} in solution decreased continuously and almost was consumed eventually. The experimental results indicated that ACC nanoparticles were successfully precipitated in 10 mM calcium salts–ethanol solution when reaction time was 4 h, which were then used for subsequent analysis.

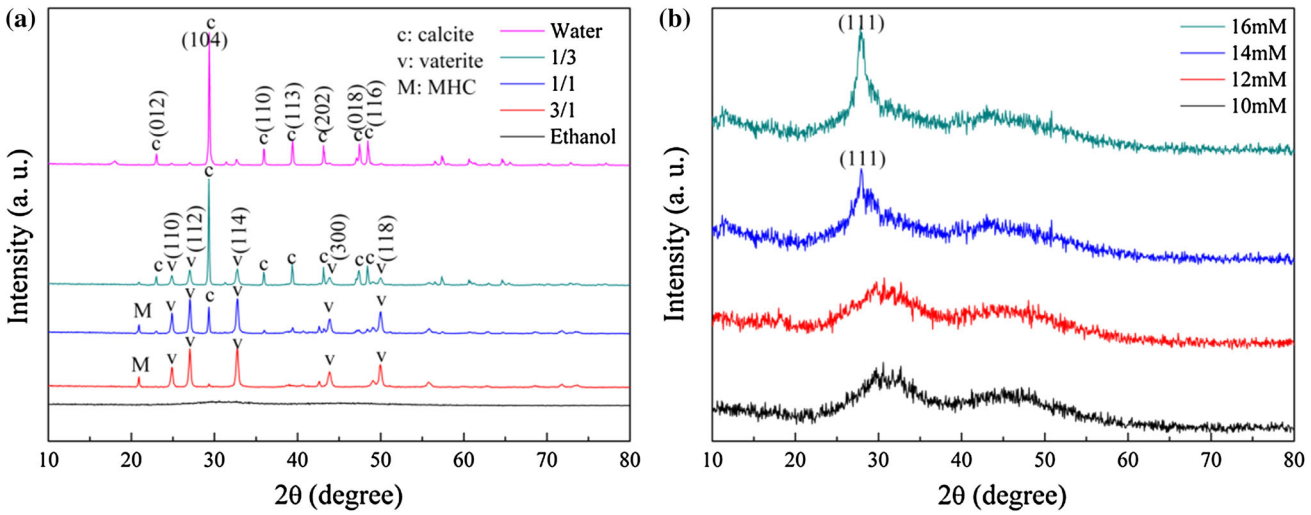

Figure 2 XRD patterns of ACC nanoparticles synthesized in: **a** water, ethanol, mixture of water and ethanol with volume ratio of 3/1, 1/1 and 1/3, **b** calcium salts solution with different concentrations: 10, 12, 14 and 16 mM.

Table 1 Particle size of ACC prepared at different reaction times

Sample	Reaction time (h)	Concentration of calcium chloride (mM)	Size (nm)	Zeta potential (mV)
ACC-1	4	10	106.2	151.7
ACC-2	8	10	171	159.5
ACC-3	12	10	213.3	168.2
ACC-4	24	10	355	156.7
ACC-5	36	10	447	198.1

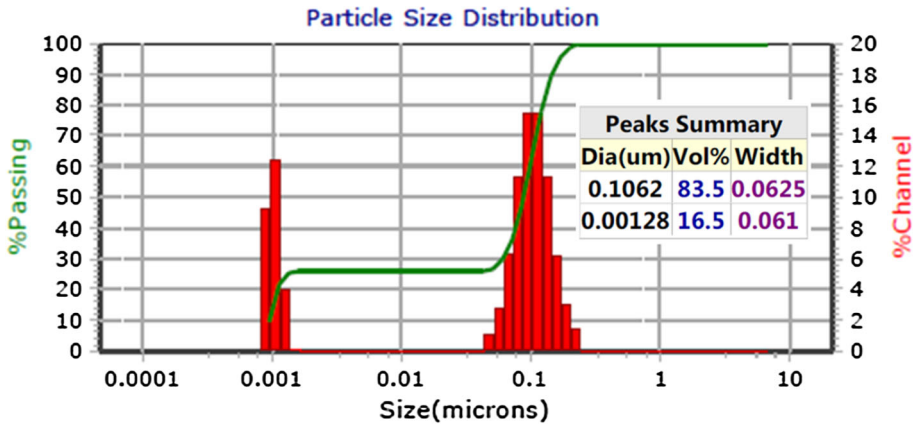

Figure 3 Particle size distribution of ACC nanoparticles measured by DLS.

Characterizations of ACC nanoparticles

Morphology

The SEM and TEM images of ACC, displayed in Fig. 5a, b, clearly show that this material was constructed from aggregation of nanoparticles. Obviously, ACC has a particle size of less than 100 nm, which was smaller than the size measured by DLS (Fig. 3). This was attributed to the fact that numerous ACC nanoaggregates were measured in aqueous solution by DLS, but the micrographs of ACC were observed in dried state [27]. The selected area electron diffraction (SAED) pattern exhibited no obvious distinct diffraction spots, indicating that these nanoparticles were amorphous. Furthermore, energy-

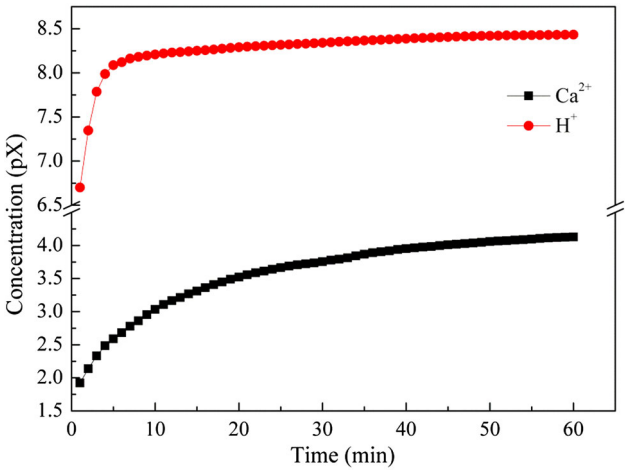

Figure 4 Tendency of pH and pCa change within the first one hour.

dispersive spectrometer (EDS, Fig. 5c) analysis showed that the resultants were indeed consisted by calcium carbonate, demonstrating that the presence of Ca, C and O in the form of ACC aggregates.

FT-IR

To further study the characteristics of amorphous phase, the FT-IR spectrum of ACC is displayed in Fig. 6. It showed the splitting peaks attributed to asymmetric stretch (v3) of C–O were observed at 1494 and 1419 cm^{-1}, which was typical characteristic of ACC. Moreover, spilt peaks located at 867 and 1075 cm^{-1} could be attributed to out-plane bending (v2) of CO_3^{2-} and symmetric stretch (v1) of C–O, respectively [13, 18]. Another characteristic IR band of ACC was without distinctive v4 band, which was consistent with the previous reports [28, 29]. In addition, the peaks at around 1634 and 3435 cm^{-1} were due to the bending and stretch vibrations of water, respectively.

N_2 adsorption–desorption isotherm

As shown in Fig. 7, Brunauer–Emmett–Teller (BET) analysis of ACC after predrying treatment at 100 °C for two hours was carried out by N_2 adsorption–desorption. The BET surface area and pore volume were approximately 173 $m^2\ g^{-1}$ and 0.59 $cm^3\ g^{-1}$, respectively. Moreover, the pore size distribution (PSD) calculated using density function theory was relatively narrow, with an average pore size around 13.9 nm. According to the previous studies, the capillary force and surface free energy caused by nanoporous structure could result in a high drug loading,

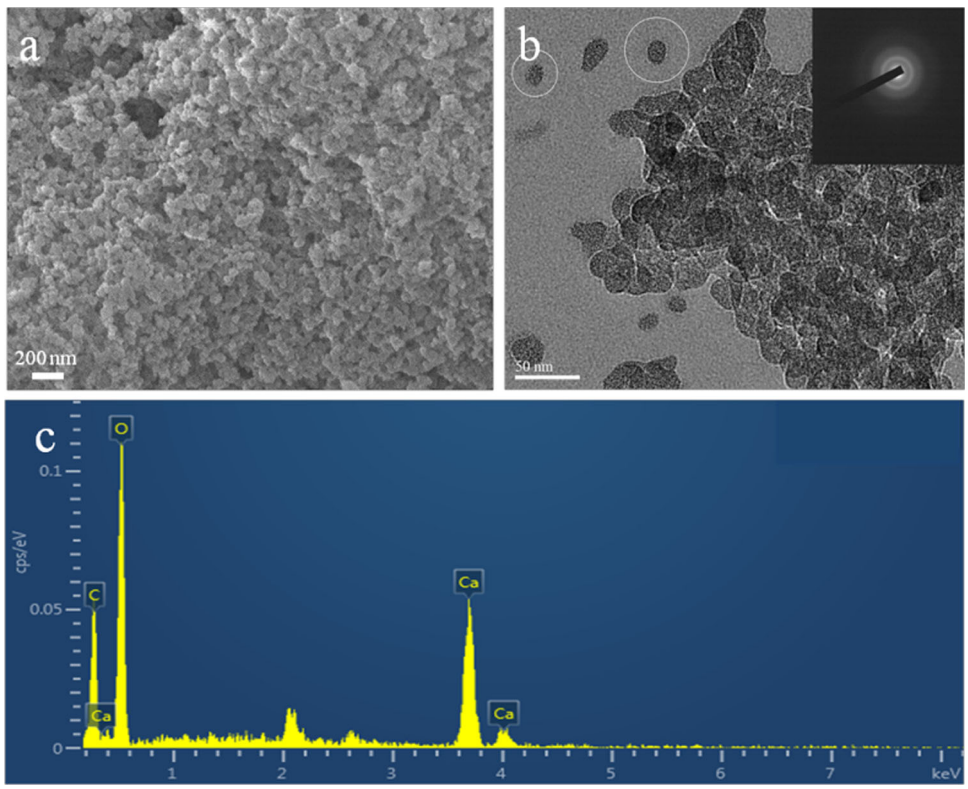

Figure 5 **a** SEM, **b** TEM and **c** EDS micrographs of ACC nanoparticles precipitated in 10 mM calcium salts ethanol solution when reaction time was 4 h.

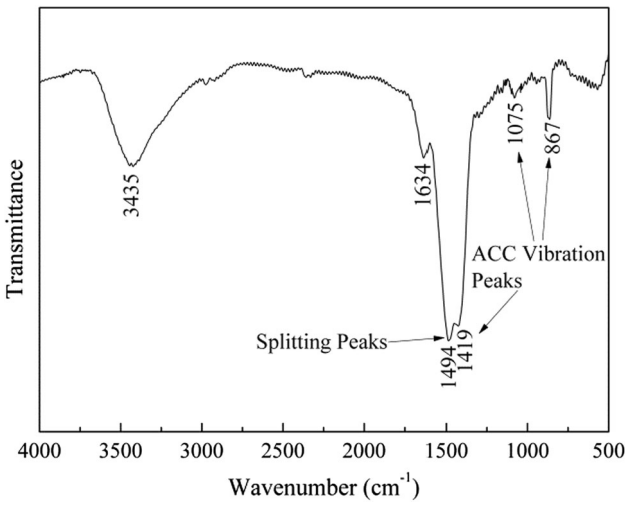

Figure 6 FT-IR spectrum of ACC nanoparticles.

which provided an opportunity to apply ACC as a potential carrier [12, 30].

TG

The thermal behavior of ACC and crystalline calcium carbonate was analyzed by TG (Fig. 8). Single-step decomposition with mass loss value of 41% was observed for crystalline calcium carbonate at temperatures higher than 650 °C, corresponding to the decomposition of calcium carbonate [31]. Three apparent weight loss processes were found in TG curves of ACC: The first could be assigned to physisorbed water release (from beginning to 230 °C); the second was attributed to the loss of structural water (230–350 °C); and the third could be explained by decomposition of calcium carbonate (above 350 °C) [32, 33]. Accordingly, it could be estimated that the amount of water involved in ACC nanoparticles was about 18% and the weight loss ratio of calcium carbonate to water was around 1.89. Thus, it was indicated that ethanol could effectively retarded the dynamics of phase transformations of ACC, which provides a broadened space for drug loading and release.

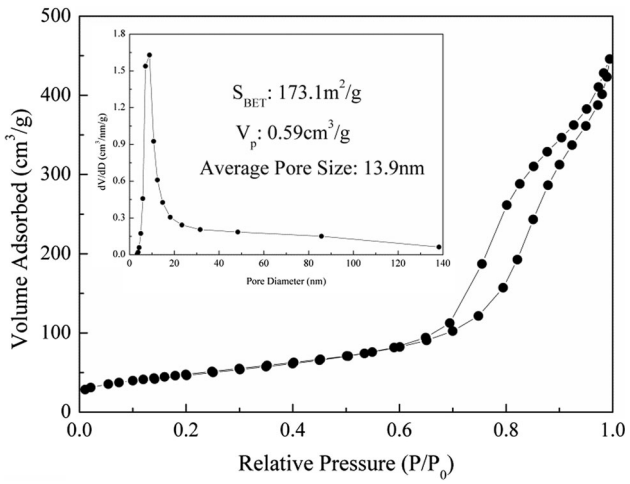

Figure 7 N_2 adsorption–desorption isotherm and pore size distribution (inset) of ACC nanoparticles.

Cur loading and release properties of ACC nanoparticles

Due to the capillary force caused by nanoporous structure, ACC nanoparticles could provide high loading capacity of drugs regardless of their hydrophilicity [12, 30, 34]. In this study, the solubility of Cur in ethanol enables it to be encapsulated readily in ACC particles. As expected, the loading capacity and entrapment efficiency of Cur were found to be 19.2 ± 1.48 wt% and 45.32 ± 2.31 wt%, respectively. Besides drug loading, the release behavior is another significant factor for evaluating a drug carrier. It is well known that the extracellular pH in tumor is about 4–6 and extracellular pH of normal tissue and blood is approximately 7.4 [35]. Therefore, the drug release profiles of ACC-Cur were investigated in PBS buffer (pH 5.4 and 7.4). As shown in Fig. 9, around 65.83% of Cur was released out within 11 h at acidic pH (5.4), while only around 51.28% of Cur was released from ACC-Cur within the same time at neutral pH (7.4). As we know, these results could be attributed to the acid sensitivity of calcium carbonate

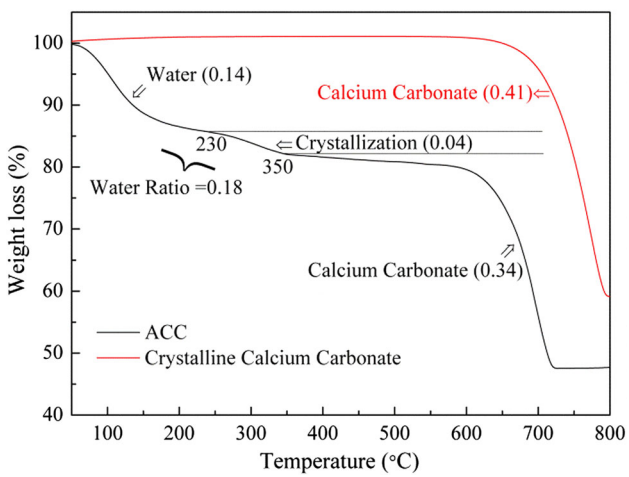

Figure 8 TG curves of ACC and crystalline calcium carbonate.

[36]. Furthermore, Cur release behavior is indirectly affected due to crystallization of ACC [37]. Therefore, ACC nanoparticles were effective to control the release of Cur, thereby increasing Cur availability and prolonging circulation time.

Antioxidant analysis

To evaluate the bioactivity, DPPH and $ABTS^{\cdot+}$ radicals were employed to test the antioxidant capacity of Cur, ACC-Cur and released Cur. It was clear that the antioxidant effectiveness for all samples was enhanced in a concentration-dependent manner (Fig. 10). In 12 μg mL^{-1} samples solution, DPPH scavenging capacities of free Cur and released Cur were about 48.12% and 41.01%, respectively, while the scavenging capacity was 33.12% for ACC-Cur, revealing a lower antioxidant activity. A similar phenomenon was seen on the determination of $ABTS^{\cdot+}$ radical scavenging activity. Obviously, the weak scavenging capacity of ACC-Cur was attributed to the envelopment of Cur. As expected, the Cur released from ACC-Cur has the same antioxidant effectiveness as free Cur, which was consistent with the previous study [21]. Therefore, it was helpful to prolong antioxidation time of Cur by sustained release ACC nanoparticles, which provides a broadened space for applications in food field.

Cur protection

It has been reported that there are a various factors such as temperature, light, pH and UV radiation to affect the chemical stability of Cur [38]. Accordingly, the ACC-loading strategy for preventing the decomposition of Cur has a profound significance in the drug delivery. For free Cur, the DPPH radical scavenging capacity (Fig. 11) reduced from 48.12% to 28.27, 32.84, 25.13 and 29.47% when the samples suffered from 60 °C treatment for 30 min, fluorescent lamp irradiation for 1 h, daylight irradiation for 1 h and UV radiation for 1 h, respectively. The drastically reduced antioxidant activity of treated-Cur was consistent with the previous studies [20, 23]. By contrast, Fig. 11 shows that the DPPH radical scavenging capacity of encapsulated Cur reduced from 46.33% to 41.61, 43.28, 36.02 and 39.46% when the samples suffered from the same treatment, respectively. The results indicated that Cur could be effectively protected by nano-sized ACC, which was significant to broaden Cur applications in cancer treatment.

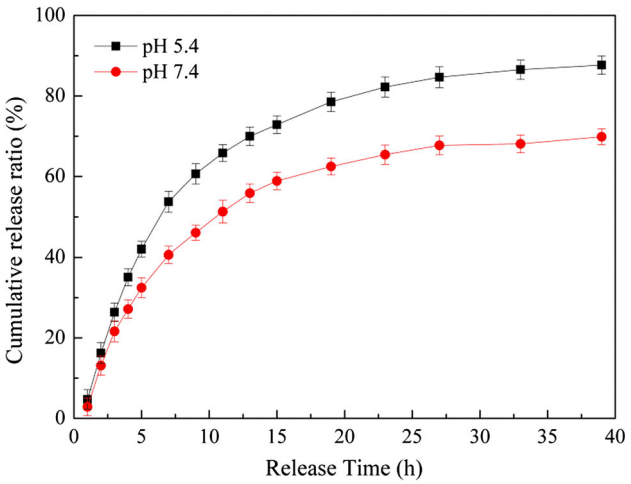

Figure 9 Drug release profiles of Cur-loaded ACC in PBS buffer (pH 5.4 and 7.4).

Cytotoxicity tests

To further evaluate whether the as-prepared ACC can be used as a potential drug carrier, A549 cells were selected to determine the toxicity of these nanoparticles. As shown in Fig. 12, there was an inconspicuous change in cell viability (over 80%) for samples containing ACC particles, which indicated that a harmfulness drug carrier was successfully synthesized. By contrast, the viability of cells co-cultured with ACC-Cur was decreased in a concentration-dependent manner. The cells remained only 45% viable when the concentration of ACC-Cur was 32 μg mL^{-1}. This phenomenon was also reported in the previous works [9, 16]. The results suggested that ACC nanoparticles have pleasurable biocompatibility, and as-prepared ACC-Cur was significant for the damaging of cancer cells.

Conclusion

In summary, the "pure" ACC nanoparticles that applied as a drug carrier for curcumin (Cur) delivery were successfully precipitated in absolute ethanol by a simple vapor diffusion method. The as-obtained material exhibited a relatively narrow size distribution located at approximately 100 nm when the reaction time was 4 h. The BET surface area, pore volume and pore size of water-containing resultants were approximately 173 m^2 g^{-1}, 0.59 cm^3 g^{-1} and

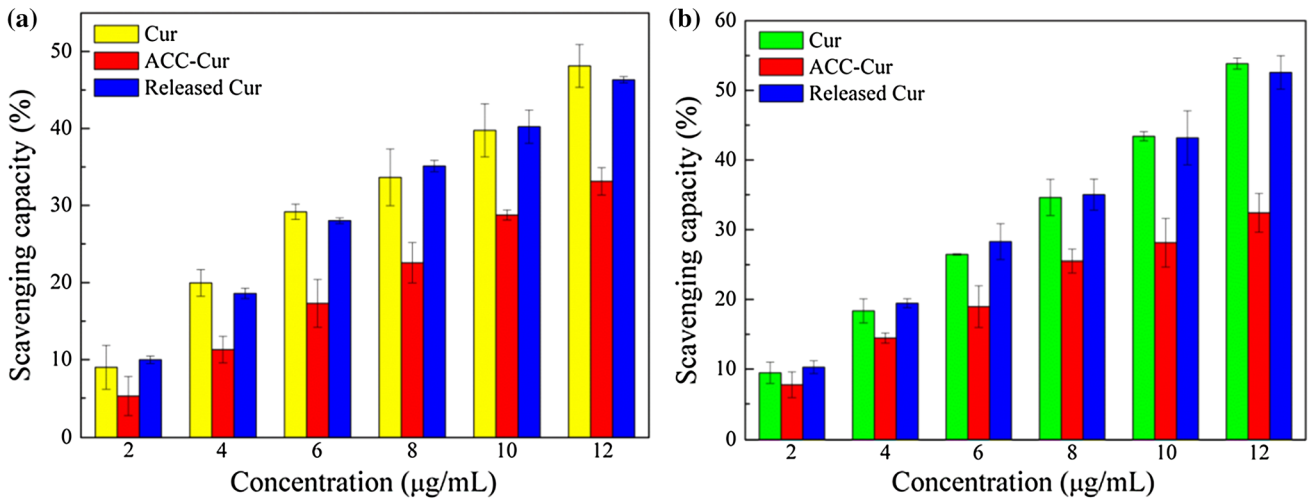

Figure 10 **a** DPPH and **b** $ABTS^{\cdot+}$ radical scavenging capacity of Cur, ACC-Cur and released Cur.

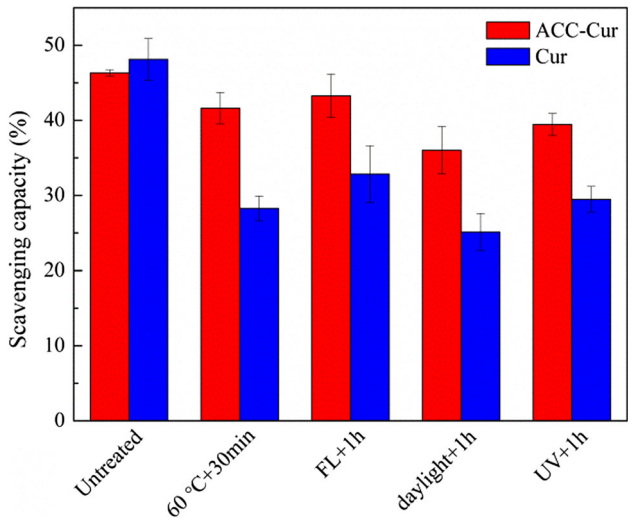

Figure 11 Cur protection by ACC nanoparticles in different treatments.

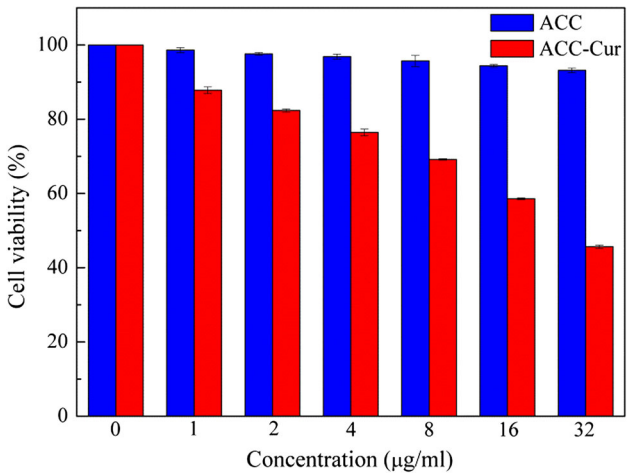

Figure 12 Cytotoxicity test of ACC and ACC-Cur using A549 cells. The data were given as mean ± standard deviation (SD) based on the measurements of the samples from three branches.

13.9 nm, respectively, indicating that the nano-sized ACC has high surface free energy to promote the loading of small molecules. Meanwhile, in vitro release manifested that ACC could effectively control the release of Cur (over 40 h) in PBS buffer (pH 5.4 and 7.4). When the concentration of Cur was 12 μg mL^{-1}, for pure Cur and released Cur, the radicals scavenging capacity was over 40%. The ACC nanoparticles also showed a significant ability to protect Cur in different treatments. Moreover, nano-sized ACC has pleasurable biocompatibility, and the as-prepared ACC-Cur was significant for the damaging of A549 cells. Therefore, the stable and pure ACC could provide an ideal carrier for drug delivery.

Acknowledgements

The work was financially supported by the Scientific and Technological Innovation Programs of Higher Education Institutions in Shanxi (172040098-S), National Natural Science Foundation of China (31700689, 51502192), International Cooperation Project Foundation of Shanxi Province in China (201803D421076), and the Fund Program for the Scientific Activities of Selected Returned Overseas Professionals in Shanxi Province.

Compliance with ethical standards

Conflict of interest The authors declare that they have no conflict of interest.

References

[1] Kelly ML, Benzel EC (2015) Surgery versus radiation therapy alone in treating spinal metastasis: a perspective. World Neurosurg 83:1020–1021

[2] Mcelwain TJ, Peckham MJ (1974) Blood and neoplastic diseases: management of solid tumours-surgery, radiotherapy, and chemotherapy. Br Med J 4:645–647

[3] Kaliki S, Shields CL (2015) Retinoblastoma: achieving new standards with methods of chemotherapy. Ind J Ophthalmol 63:103–109

[4] Salman D, Barton S, Gebara SN (2014) Improving the stability of anticancer drugs. J Oncol Pharm Pract Off Publ Int Soc Oncol Pharm Pract 20:236

[5] Bardin C, Astier A, Vulto A, Sewell G, Vigneron J, Trittler R, Daouphars M, Paul M, Trojniak M, Pinguet F (2011) Guidelines for the practical stability studies of anticancer drugs: a European consensus conference ☆. Annal Pharm Franç 69:221–231

[6] Závišová V, Koneracká M, Múčková M, Kopčanský P, Tomašovičová N, Lancz G, Timko M, Pätoprstá B, Bartoš P, Fabián M (2009) Synthesis and characterization of polymeric nanospheres loaded with the anticancer drug paclitaxel and magnetic particles. J Magn Magn Mater 321:1613–1616

[7] Riaz MK, Riaz MA, Zhang X, Lin C, Wong KH, Chen X, Zhang G, Lu A, Yang Z (2018) Surface functionalization and targeting strategies of liposomes in solid tumor therapy: a review. Int J Mol Sci 19:195

[8] Zhou B, Wu B, Wang J, Qian Q, Wang J, Xu H, Yang S, Feng P, Chen W, Li Y, Jiang J, Han B (2018) Drug-mediation formation of nanohybrids for sequential therapeutic delivery in cancer cells. Coll Surf B Biointerfaces 163:284–290

[9] Tolba E, Muller WEG, El-Hady BMA, Neufurth M, Wang X (2015) High biocompatibility and improved osteogenic potential of amorphous calcium carbonate/vaterite. J Mater Chem B 4:376–386

[10] Zhang Y, Ma P, Wang Y, Du J, Zhou Q, Zhu Z, Yang X, Yuan J (2012) Biocompatibility of porous spherical calcium carbonate microparticles on hela cells. World J Nano Sci Eng 2:25–31

[11] Lauth V, Maas M, Rezwan K (2017) An evaluation of colloidal and crystalline properties of $CaCo_3$ nanoparticles for biological applications. Mater Sci Eng C Mater Biol Appl 78:305–314

[12] Sun R, Zhang P, Bajnoczi EG, Neagu A, Tai CW, Persson I, Stromme M, Cheung O (2018) Amorphous calcium carbonate constructed from nanoparticle aggregates with unprecedented surface area and mesoporosity. ACS Appl Mater Interfaces 10:21556–21564

[13] Hu Y, Zhou Y, Xu X, Tang R (2015) Phase-controlled crystallization of amorphous calcium carbonate in ethanol-water binary solvents. Cryst Res Technol 50:312–318

[14] Koga N, Nakagoe Y, Tanaka H (1998) Crystallization of amorphous calcium carbonate. Thermochim Acta 318:239–244

[15] Ihli J, Wong WC, Noel EH, Kim YY, Kulak AN, Christenson HK, Duer MJ, Meldrum FC (2014) Dehydration and crystallization of amorphous calcium carbonate in solution and in air. Nat Commun 5:3169

[16] Peng Y, Sun HY, Wang ZC, Xu XD, Song JC, Gong ZJ (2016) Fabrication of alginate/calcium carbonate hybrid microparticles for synergistic drug delivery. Chemotherapy 61:32–40

[17] Wang J, Yong K, Feng L, Dan S, Tao Y, Yong Q (2018) Construction of ph-responsive drug delivery platform with calcium carbonate microspheres induced by chitosan gels. Ceram Int 44:7902–7907

[18] Chen SF, Colfen H, Antonietti M, Yu SH (2013) Ethanol assisted synthesis of pure and stable amorphous calcium carbonate nanoparticles. Chem Commun 49:9564–9566

[19] Sunagawa Y, Katanasaka Y, Hasegawa K, Morimoto T (2015) Clin Appl Curcumin Pharm 3:131–135

[20] Xia G, Wenfeng L, Heping W, Yan-Ying F, Huifang W, Xianghua G, Baolong N, Xuechen G (2018) Preparation, characterization, release and antioxidant activity of curcumin-loaded amorphous calcium phosphate nanoparticles. J Non Cryst Solids 500:317–325

[21] O'Toole MG, Soucy PA, Chauhan R, Raju MV, Patel DN, Nunn BM, Keynton MA, Ehringer WD, Nantz MH, Keynton RS, Gobin AS (2016) Release-modulated antioxidant activity of a composite curcumin-chitosan polymer. Biomacromol 17:1253–1260

[22] Khanji AN, Michaux F, Petit J, Salameh D, Rizk T, Jasniewski J, Banon S (2018) Structure, gelation, and antioxidant properties of curcumin-doped casein micelle powder produced by spray-drying. Food Funct 9:971–981

[23] Wang H, Gong X, Guo X, Liu C, Fan YY, Zhang J, Niu B, Li W (2019) Characterization, release, and antioxidant activity of curcumin-loaded sodium alginate/zno hydrogel beads. Int J Biol Macromol 121:1118–1125

[24] Koga N, Yamane Y, Kimura T (2011) Thermally induced transformations of calcium carbonate polymorphs precipitated selectively in ethanol/water solutions. Thermochim Acta 512:13–21

[25] Farhadi-Khouzani M, Chevrier DM, Zhang P, Hedin N, Gebauer D (2016) Water as the key to proto-aragonite amorphous $CaCo_3$. Angew Chem Int Ed Engl 55:8117–8120

[26] Konrad F, Gallien F, Gerard DE, Dietzel M (2016) Transformation of amorphous calcium carbonate in air. Cryst Growth Des 16:6310–6317

[27] Zhang X, Li L, Li C, Zheng H, Song H, Xiong F, Qiu T, Yang J (2017) Cisplatin-crosslinked glutathione-sensitive micelles loaded with doxorubicin for combination and targeted therapy of tumors. Carbohydr Polym 155:407–415

[28] Nebel H, Dr ME (2010) Continuous preparation of calcite, aragonite and vaterite, and of magnesium-substituted amorphous calcium carbonate (Mg-ACC). Z Für Anorg Allg Chem 634:1439–1443

[29] Cai AH, Xu XR, Pan HH, Tao JH, Rui L, Tang RK, Cho K (2008) Direct synthesis of hollow vaterite nanospheres from amorphous calcium carbonate nanoparticles via phase transformation. J Phys Chem C 112:11324–11330

[30] Peng C, Zhao Q, Gao C (2010) Sustained delivery of doxorubicin by porous $CaCo_3$ and chitosan/alginate multilayers-coated caco 3 microparticles. Coll Surf A Physicochem Eng Asp 353:132–139

[31] Kimura T, Koga N (2011) Monohydrocalcite in comparison with hydrated amorphous calcium carbonate: precipitation condition and thermal behavior. Cryst Growth Des 11:3877–3884

[32] Zhang J, Zhou X, Dong C, Sun Y, Yu J (2018) Investigation of amorphous calcium carbonate's formation under high concentration of magnesium: the prenucleation cluster pathway. J Cryst Growth 494:8–16

[33] Schmidt MP, Ilott AJ, Phillips BL, Reeder RJ (2014) Structural changes upon dehydration of amorphous calcium carbonate. Environ Toxicol Chem 25:1291–1297

[34] Bosio VE, Cacicedo ML, Calvignac B, Leon I, Beuvier T, Boury F, Castro GR (2014) Synthesis and characterization of $CaCo_3$-biopolymer hybrid nanoporous microparticles for controlled release of doxorubicin. Coll Surf B Biointerfaces 123:158–169

[35] Li B, Zhang XX, Huang HY, Chen LQ, Cui JH, Liu Y, Jin H, Lee BJ, Cao QR (2018) Effective deactivation of a549 tumor cells in vitro and in vivo by RGD-decorated chitosan-functionalized single-walled carbon nanotube loading docetaxel. Int J Pharm 543:8–20

[36] Goss SL, Lemons KA, Kerstetter JE, Bogner RH (2007) Determination of calcium salt solubility with changes in ph and $p(Co_2)$, simulating varying gastrointestinal environments. J Pharm Pharmacol 59:1485–1492

[37] Tobler DJ, Rodriguez-Blanco JD, Sørensen HO, Stipp SLS, Dideriksen K (2016) The effect of ph on amorphous calcium carbonate (acc) structure and transformation. Cryst Growth Des 16:4500–4508

[38] Li Q, Chen J, Luo S, Xu J, Huang Q, Liu T (2015) Synthesis and assessment of the antioxidant and antitumor properties of asymmetric curcumin analogues. Eur J Med Chem 93:461–469